Earth and Planetary Science Letters 482 (2018) 556–566

Contents lists available at ScienceDirect

Earth and Planetary Science Letters

www.elsevier.com/locate/epsl

Nitrogen evolution within the Earth's atmosphere–mantle system assessed by recycling in subduction zones

Ananya Mallik [a,*], Yuan Li [b], Michael Wiedenbeck [c]

[a] Bayerisches Geoinstitut, Universität Bayreuth, 95440 Bayreuth, Germany
[b] State Key Laboratory of Isotope Geochemistry, Guangzhou Institute of Geochemistry, Chinese Academy of Sciences, Guangzhou 510460, China
[c] Helmholtz Zentrum Potsdam, Deutsches GeoForschungZentrum GFZ, Telegrafenberg, 14473 Potsdam, Germany

ARTICLE INFO

Article history:
Received 4 July 2017
Received in revised form 7 October 2017
Accepted 23 November 2017
Available online 7 December 2017
Editor: T.A. Mather

Keywords:
deep nitrogen cycling
atmosphere–mantle evolution
subduction zones
solubility limit
recycled volatiles

ABSTRACT

Understanding the evolution of nitrogen (N) across Earth's history requires a comprehensive understanding of N's behaviour in the Earth's mantle – a massive reservoir of this volatile element. Investigation of terrestrial N systematics also requires assessment of its evolution in the Earth's atmosphere, especially to constrain the N content of the Archaean atmosphere, which potentially impacted water retention on the post-accretion Earth, potentially causing enough warming of surface temperatures for liquid water to exist. We estimated the proportion of recycled N in the Earth's mantle today, the isotopic composition of the primitive mantle, and the N content of the Archaean atmosphere based on the recycling rates of N in modern-day subduction zones. We have constrained recycling rates in modern-day subduction zones by focusing on the mechanism and efficiency of N transfer from the subducting slab to the sub-arc mantle by both aqueous fluids and slab partial melts. We also address the transfer of N by aqueous fluids as per the model of Li and Keppler (2014). For slab partial melts, we constrained the transfer of N in two ways – firstly, by an experimental study of the solubility limit of N in melt (which provides an upper estimate of N uptake by slab partial melts) and, secondly, by the partitioning of N between the slab and its partial melt. Globally, 45–74% of N introduced into the mantle by subduction enters the deep mantle past the arc magmatism filter, after taking into account the loss of N from the mantle by degassing at mid-ocean ridges, ocean islands and back-arcs. Although the majority of the N in the present-day mantle remains of primordial origin, our results point to a significant, albeit minor proportion of mantle N that is of recycled origin ($17 \pm 8\%$ or $12 \pm 5\%$ of N in the present-day mantle has undergone recycling assuming that modern-style subduction was initiated 4 or 3 billion years ago, respectively). This proportion of recycled N is enough to cause a departure of N isotopic composition of the primitive mantle from today's $\delta^{15}N$ of $-5‰$ to $-6.8 \pm 0.9‰$ or $-6.3 \pm 1.2‰$. Future studies of Earth's parent bodies based on the bulk Earth N isotopic signature should take into account these revised values for the $\delta^{15}N$ composition of the primitive mantle. Also, the Archaean atmosphere had a N partial pressure of 1.4–1.6 times higher than today, which may have warmed the Earth's surface above freezing despite a faint young Sun.

1. Introduction

Nitrogen (N) is the most abundant element in the Earth's present atmosphere; nonetheless, given recent estimates, the most massive reservoir for N is likely the mantle, which contains between 2 and 10 times the atmosphere's N mass (Johnson and Goldblatt, 2015). Therefore, understanding Earth's N systematics requires a thorough investigation of N cycling between Earth's various reservoirs, including N transfer from the atmosphere to the mantle and vice-versa (Barry and Hilton, 2016; Busigny et al., 2011; Goldblatt et al., 2009; Mikhail and Sverjensky, 2014). A fundamental question about N in the Earth's mantle is whether it is of primordial or of recycled origin (Marty and Dauphas, 2003). The answer to this question has two key implications. Firstly, N content and isotopic composition of the primitive mantle (i.e., during the first billion years of Earth history) is key for estimating the nature and proportion of the parent bodies that accreted to form the Earth (Cartigny and Marty, 2013; Li et al., 2016). Isotopic compositions of fibrous diamonds and mid-ocean ridge basalts show that the present-day mantle (mostly the upper mantle) has a $\delta^{15}N$ $[(^{15}N/^{14}N)_{sample}/(^{15}N/^{14}N)_{air}-1)\times 1000]$ value of $-5 \pm 2‰$

* Corresponding author.
E-mail address: Ananya.Mallik@uni-bayreuth.de (A. Mallik).

https://doi.org/10.1016/j.epsl.2017.11.045
0012-821X/

(Cartigny and Marty, 2013). Given that both Archaean as well as younger sediments are enriched in ^{15}N (Cartigny and Marty, 2013), presence of recycled crustal material in the mantle would imply that the primitive mantle was depleted in ^{15}N as compared to the present-day mantle. If such is the case, it would imply that the Earth might have dominantly accreted from reduced enstatite chondrites, rather than oxidized carbonaceous chondrites (Javoy, 1997; Li et al., 2016). Secondly, if it can be shown that there has been a drawdown of N from the atmosphere to the mantle via subduction, then estimating the mass of subduction-derived N in the present-day mantle can be used to constrain the partial pressure of N in the Archaean atmosphere. A high partial pressure of N in the Archaean atmosphere could have caused warming in the early Earth in spite of a faint young Sun (Goldblatt et al., 2009), because it would enhance the potency of greenhouse gases by pressure broadening their absorption lines. Also, a N-rich Archaean atmosphere is purported to help retain water which could be a key requirement for development of the Earth into a wet planet, as we know it today (Wordsworth and Pierrehumbert, 2014).

The isotopic composition of N in the primitive mantle remains largely unknown and the partial pressure of N in the Archaean atmosphere is debated. A recent model based on the isotopes of N–He–Ne–Ar in oceanic basalts predicts a 50% higher N partial pressure in the Archaean atmosphere than that at present (Barry and Hilton, 2016). This, however, contradicts results obtained from analysing fluid inclusions from Archaean hydrothermal quartz (Marty et al., 2013), raindrop size distribution (Som et al., 2012) and vesicle size distribution (Som et al., 2016) preserved in Archaean rocks, all of which yielded an Archaean atmospheric N partial pressure of ~0.5 bar (which is lower than today). Here, to constrain the mass and isotopic composition of N in the primitive mantle, from which we can derive the N partial pressure in the Archaean atmosphere, we performed a systematic study on N recycling efficiency (or the proportion of the subducted nitrogen that escapes slab dehydration and/or melting and enters the deep Earth) in modern subduction zones.

Previous studies have estimated modern-day N recycling efficiency based on the difference between ingassing rates in subduction zones and degassing rates at arcs, mid-ocean ridges, ocean islands and back arc spreading centres. Such studies have estimated that 0% (Fischer et al., 2002) to 80–92% (e.g. Barry and Hilton, 2016; Busigny et al., 2011) of slab N is transported to mantle depths beyond sub-arc conditions. Key to estimating recycling rates of an element using such an approach is the assumption that the entire mass of the element carried away from the subducted slab is degassed at arcs; this assumption is not necessarily valid for N. For example, xenoliths from the mantle-wedge, the lithosphere and the lower crust of overriding plates contain abundant amphibole and/or mica (e.g. Kawamoto et al., 2013), which can incorporate significant amounts of N in the form of NH_4^+ substituting for K^+. The shallow upper mantle, such as the sub-arc mantle, can also store 5–20% of present day atmospheric N (Li et al., 2013) during its metasomatism by siliceous slab-derived flux. Hence, the assumption that the flux of N degassed at arcs represents the entire flux released from the subducted slab results in an overestimation of the rates of N sent past the "arc filter" into the deep mantle. Furthermore, while the outflux/degassing rate of N at arcs is constrained (Hilton et al., 2002), differences in the estimates of the influx of N can yield very different estimates of deep mantle injection rates, as has been observed in previous studies (e.g. Busigny et al., 2011; Fischer et al., 2002).

Here, we used an innovative forward approach for determining recycling efficiency in subduction zones, by focusing on the extraction of N from the slab to the overlying mantle-wedge via aqueous fluids and slab partial melts, for which we have investigated a broad range of subduction thermal regimes (Syracuse et al., 2010). We estimated the N ingassing rate for each of the Earth's 55 subduction zones (Supplementary Table 1). Then we determined the rate of N transfer by aqueous fluids in each subduction zone taking into account pressure (P), temperature (T) and oxygen fugacity (fO_2) along the slab-top while also considering the likely N speciation in subduction zone fluids (Li and Keppler, 2014) (Supplementary Information). For subduction zones where slabs are hot enough to partially melt, we quantified the rate of N transported by slab partial melts (referred to as slab-melts) using two approaches, assuming – (i) N is dissolved in the slab-melt at its solubility limit, which anchors the highest rate of N removal from the slab, and (ii) N partitioning between the slab and slab-melt is controlled by NH_4^+, and NH_4^+ behaves similarly as Rb^+ due to the same charge and similar ionic radii; hence, the behaviour of Rb^+ was used as a guide to the partitioning of N between the key N hosting minerals in the slab and any associated partial melt.

We determined the solubility limit of N in slab-melts experimentally. The breakdown of NH_4^+-bearing minerals in the slab, such as phengite and amphibole, controls N release from the subducted slab to any resulting partial melt. N concentrations in the sediments range from 424 μg/g (Busigny et al., 2011) to 2382 μg/g (Li and Bebout, 2005). Assuming a partitioning behaviour of NH_4^+ that is similar to Rb^+ (also assuming a phengite modal abundance in sediments and modal proportion during partial melting), low degree slab partial melts should carry 0.2 to 1.1 wt.% (g/100 g) of N. We deemed it necessary to assess whether such high concentrations of N being dissolved in slab-melts are realistic, leading us to determine experimentally the solubility limit of N in slab partial melts. We also required a knowledge of (i) speciation of N at the relevant conditions, as this determines the solubility mechanism, and (ii) the effect of solubility on variable H_2O concentrations in the slab-melt (as H_2O is the principle volatile species in slab-melts whose contents can vary depending on the degree of melting, and amount of H_2O present in the slab). Considering the aforementioned factors, we experimentally determined the solubility limit of N (the concentration of N dissolved in the melt in the presence of a N-rich fluid phase) in rhyolitic slab partial melts with two different H_2O concentrations (referred to as "low H_2O" and "high H_2O" slab melts, respectively) at fO_2 and pressure conditions applicable for subduction zones (Supplementary Table 2).

2. Methods

2.1. Experimental determination of N dissolved in slab-melt at its solubility limit and analysis of experimental products

We experimentally determined N solubility limit in slab-derived partial melts. The experiments were performed at 1050–1300 °C, 2–4 GPa, fO_2 varying from ΔNNO −0.6 to −4 log units, with slab partial melts (hydrous rhyolites) containing 2.5–6.2 wt.% added N and 4 wt.% ('low H_2O slab melt') and 8 wt.% ('high H_2O slab melt') added H_2O (Table 1). These P–T conditions are appropriate for the hot core of the mantle-wedge in the sub-arc region (Syracuse et al., 2010), where the slab-melt retains its chemistry from the slab-top to the mantle-wedge by channelized flow (Pirard and Hermann, 2015), or slab-melts are produced in the mantle-wedge by the partial melting of slab lithologies in a diaper (e.g. Nielsen and Marschall, 2017). Further details about synthesis of starting materials are provided in the Supplementary Information.

We performed the experiments using a modified double capsule geometry, with $Pt_{95}Rh_5$ capsules (2.5 mm OD, 2.0 mm ID, 5.0 mm length) placed inside nickel outer capsules (5.0 mm OD, 3.0 mm ID, 10.0 mm length). Nickel oxide and distilled water were then added to the space between the inner and outer capsules. Details about the modified double capsule geometry are described in the Supplementary Information. Also, most of our experiments

Table 1
List of solubility experiments.

Experiment No.	B994	B989	A875	A799	B970	A838	B995	A870	B967	A876
P (GPa)	2	3	4	2	2	2	2	3	4	4
T (°C)	1300	1300	1300	1050	1200	1300	1300	1300	1300	1300
H_2O, N added (wt.%)	4, 3.0	4, 3.0	4, 3.0	8, 1.3	8, 2.5	8, 2.5	8, 6.2	8, 6.2	8, 2.5	8, 6.2
Duration (hr)	43	49	49	52	41	71	66	48	63	68
SiO_2	68.7(6)	67.9(2)	67.7(8)	63.3(3)	66.8(7)	67.4(4)	64.4(3)	64.3(3)	64.9(2)	63.4(8)
TiO_2	0.23(3)	0.22(3)	0.23(2)	0.19(3)	0.25(3)	0.30(3)	0.20(2)	0.21(2)	0.24(3)	0.23(3)
Al_2O_3	13.9(1)	13.58(9)	13.8(1)	16.7(1)	12.1(1)	11.31(8)	13.7(1)	13.8(1)	12.59(7)	13.78(1)
FeO	0.01(1)	0.01(1)	0.03(2)	0.21(2)	0.03(2)	0.04(2)	0.01(1)	0.03(2)	0.21(2)	0.01(1)
MnO	0.02(1)	0.01(1)	0.02(2)	0.03(2)	0.03(2)	0.03(2)	0.02(2)	0.03(2)	0.04(2)	0.01(1)
MgO	0.23(1)	0.25(2)	0.23(2)	0.26(1)	0.23(2)	0.23(2)	0.25(2)	0.26(2)	0.22(2)	0.26(2)
CaO	1.10(4)	1.10(4)	1.07(3)	1.12(3)	1.05(4)	1.11(3)	1.06(3)	1.07(4)	1.04(3)	1.06(3)
Na_2O	6.1(4)	6.0(1)	6.0(5)	6.1(2)	5.5(5)	5.4(7)	5.2(5)	5.45(1)	5.1(1)	5.4(4)
K_2O	2.41(4)	2.40(5)	2.43(7)	2.38(4)	2.48(9)	2.29(4)	2.36(5)	2.38(4)	2.19(4)	2.39(5)
P_2O_5	0.06(3)	0.06(4)	0.08(3)	0.06(3)	0.09(3)	0.10(4)	0.03(3)	0.05(3)	0.10(3)	0.03(2)
H_2O[a]	7.1(6)	8.3(3)	8.1(7)	9.6(2)	11.3(7)	11.8(6)	12.6(4)	12.2(4)	13.2(3)	13.3(8)
N^{EMPA}	0.4(2)	0.9(3)	1.0(4)	0.5(2)	0.4(2)	0.5(3)	0.4(2)	1.0(4)	0.9(3)	0.5(3)
N^{SIMS}	0.8(2)	0.9(3)	1.0(4)	–	0.5(2)	0.6(2)	0.4(1)	0.8(3)	–	0.4(2)
$X^{N_2}_{fluid}$	0.7(1)	0.32(7)	0.24(8)	0.5(2)	0.47(7)	0.90(5)	0.85(3)	0.44(4)	0.50(1)	0.83(4)
$X^{H_2O}_{fluid}$	0.29(8)	0.68(7)	0.76(8)	0.5(1)	0.53(6)	0.10(3)	0.15(2)	0.56(3)	0.50(7)	0.17(2)
$\log fO_2$ (ΔNNO)	−2.4(9)	−0.8(2)	−0.6(2)	−1.5(8)	−1.3(3)	−4(1)	−3.8(4)	−1.1(1)	−1.4(4)	−3.6(5)
$\ln(K)$	−17.8(4)	−19.5(4)	−21.5(5)	−18.7(4)	−18.2(4)	−18.3(3)	−18.6(4)	−19.9(4)	−22.4(2)	−23.4(4)
c^{OH^-} at $T_{experiment}$	4.5	5.2	4.8	8.2	8.7	8.9	10.2	8.8	11.7	10.6
$c^{H_2O}_m$ at $T_{experiment}$	0.2	0.3	0.3	7.8	1.1	0.9	1.3	0.9	1.7	1.4
c^{OH^-} at 400 °C	2.5	2.7	2.6	1.6	3.8	3.8	4.1	3.8	4.5	4.3
$c^{H_2O}_m$ at 400 °C	2.4	2.9	2.5	5.0	6.0	6.0	7.3	6.0	8.9	7.8

All concentrations are reported in wt.% (g/100 g);
[a] H_2O concentration calculated by the difference between 100 and the sum of oxides and N; $X^{N_2}_{fluid}$ and $X^{H_2O}_{fluid}$ are the mole fractions of N_2 and H_2O in the fluid phase coexisting with glass in the experiments; c^{OH^-} and $c^{H_2O}_m$ refer to concentrations of hydroxyl and molecular H_2O in the melt/glass respectively, calculated as mentioned in Supplementary Information; 400 °C is the lower limit of glass transition for rhyolite; ±1sd uncertainties mentioned in brackets and reported as least digits cited, e.g. 68.7(6) to be read as 68.7±0.6 wt.%; $\log fO_2$ is calculated based on the fluid composition coexisting with glass.

were performed isothermally across the pressure range in order to investigate the effect of pressure on the solubility of nitrogen in slab melts without any temperature influence. We also studied the temperature effect on solubility, allowing solubility values applicable at the slab-top to be investigated.

Our experiments were performed in end-loaded piston-cylinder devices at the Bayerisches Geoinstitut using talc–pyrex assemblies, tapered graphite heaters, Al_2O_3 spacers and capsule sleeves. The temperature in the experiments was monitored using a S-type thermocouple with a ±10 °C uncertainty. These experiments were run for 43–71 hr, after which the samples were quenched to room temperature by cutting off electrical power. In order to suppress formation of tiny quench bubbles due to instantaneous pressure loss, we performed isobaric quenching by manually keeping the pressure steady around the target value. Following this, the assemblies were decompressed over a period of 1–3 hr, removed from the press and polished as explained in the Supplementary Information.

We determined the speciation of N in the experimental glasses using Raman spectroscopy. The major and minor element compositions of the glasses were measured using electron microprobe analysis (EMPA). N concentrations in the glasses were measured using both EMPA and Secondary Ion Mass Spectrometry (SIMS). The details of the analytical procedures are described in the Supplementary Information.

3. Results

3.1. Experimental derivation of N speciation, mechanism of dissolution and solubility in slab-melts

The N concentrations in slab-melts coexisting with a N-rich fluid phase (Fig. 1) were measured by electron microprobe (EMPA) and secondary-ion mass spectrometer (SIMS) (Supplementary Information; Fig. 2); as expected these data-sets show a good correlation (Fig. 2b). As the SIMS data-set has much lower background corrections and better repeatability, the N concentration measured by SIMS will be used henceforth.

Raman spectra of the solubility experiments show that molecular N_2 is the dominant N species in hydrous slab-melts at the P–T–fO_2 conditions of this study (Fig. 3a, Supplementary Information). The splitting of N_2 peaks in the Raman spectra due to variable isotopic pairs is explained in the Supplementary Information. Molecular N_2 occupies ionic porosity within the melt structure, where ionic porosity is defined as $(V_m - V_i)/V_i \times 100$ (V_m = volume of melt, V_i = volume occupied by ions). The mechanism of dissolution is potentially similar to that of charge neutral species such as noble gases, carbon dioxide and molecular hydrogen in silicate melts (Carroll and Stolper, 1993; Hirschmann et al., 2012). The dependence of N solubility on concentration and speciation of H_2O in slab-melts, along with the impact of any change in H_2O speciation due to glass transition is discussed in the Supplementary Information.

Assuming that N is present in the fluid phase as N_2, similar to how it is dissolved in the slab-melt, the following equations describe the equilibrium between N in the fluid and melt phases:

$$N_2\ (\text{fluid}) = N_2\ (\text{melt}) \quad (1)$$

$$K = \frac{X^{melt}_{N_2}}{f^{fluid}_{N_2}} \quad (2)$$

where K = equilibrium constant, $X^{melt}_{N_2}$ = mole fraction of N in the slab-melt, $f^{fluid}_{N_2}$ = fugacity of N in the fluid. The estimation of N fugacity (fN_2) in the fluid phase is discussed in the Supplementary Information. We developed a solubility model for N in rhyolitic

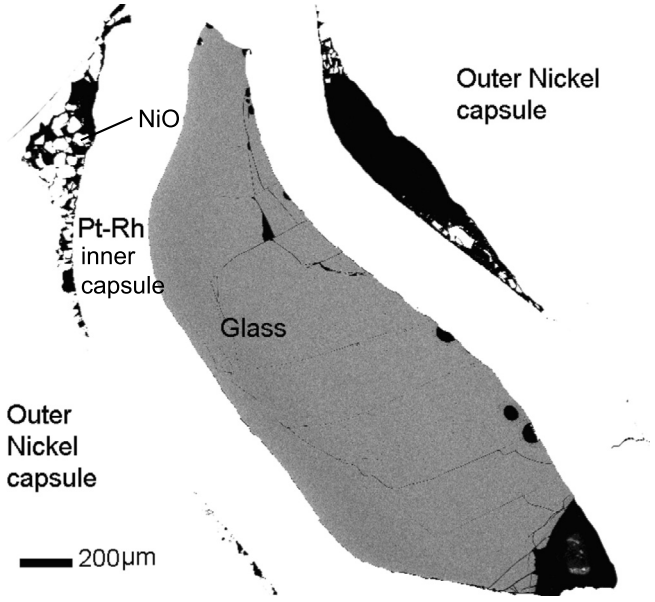

Fig. 1. Backscattered electron image of experiment A838 (2 GPa, 1300 °C, high H_2O slab melt) performed in Pt_{95}–Rh_5 inner capsule with nickel outer capsule and NiO + H_2O placed between the two capsules. This geometry is a modified double capsule geometry to buffer the oxygen fugacity of the sample close to that given by the reaction between Ni and NiO (see main text for more details). The vesicles in the glass are remnants of nitrogen–H_2O fluids that existed with the melt during the experiments. In this study, nitrogen solubility in the melt is defined as the dissolved nitrogen concentration in the melt in the presence of nitrogen-rich fluids. Significant numbers of microbubbles (representing exsolution of volatiles during quenching) are conspicuously absent.

melt using the following thermodynamic relation, based on Equations (1) and (2):

$$\ln(K) = \ln(K_0) - \frac{\Delta H^0}{R}\left(\frac{1}{T} - \frac{1}{T_0}\right) - \frac{\Delta V^0}{RT}(P - P_0) \quad (3)$$

where K_0 = equilibrium constant at reference temperature (T_0) of 1300 °C and reference pressure (P_0) of 0.001 GPa, ΔH^0 = enthalpy at P_0 and T, ΔV^0 = volume change at P and T (also the partial molar volume of N_2 in this case) and, R = molar gas constant. Given that Ar and N_2 have very similar radii and their mechanism of incorporation in silicate melt structure is the same, it is expected that their partial molar volumes are also similar. Using the isothermal experiments at 1300 °C, we estimated the partial molar volumes for low H_2O and high H_2O slab-melts as 24.1 (±0.6) $cm^3\,mol^{-1}$ and 28.3 (±0.9) $cm^3\,mol^{-1}$, respectively (Fig. 3b), which are within the range or close to that of Ar (23–25 $cm^3\,mol^{-1}$) (Paonita, 2005).

We found no correlation between $\ln(K)$ and $1/T$ for "high H_2O slab-melt", as shown by R^2 value of 0.16 (Fig. 3c); hence, for practical purposes solubility is considered independent of temperature. This is similar to that observed for the dissolution of noble gases in silicate melts (Paonita, 2005). Rearranging Equation (3) and using the slope and y-intercept of the best-fit line for $\ln(K)$ vs $1/T$, ΔH^0 can be obtained in two ways:

1. $\Delta H^0_1 = -m \times R - \Delta V^0 \times (P - P_0)$, where, m = slope of the line relating $\ln(K)$ to $1/T$. As stated before, in this study, $m = 0$ for practical purposes, hence, $\Delta H^0_1 = -56.5(\pm 1.7)$ kJ/mol.
2. $\Delta H^0_2 = R \times T_0 \times [c - \ln(K_0)]$, where, c = y-intercept of the line relating $\ln(K)$ to $1/T$. If $m = 0$, c can be approximated to be −18.5 based on Fig. 3c. Thus, $\Delta H^0_2 = -58.7$ (±4.4) kJ/mol.

ΔH^0_1 is within 4% of ΔH^0_2. Hence, the ΔH^0 values estimated by the two methods agree with each other very well. However, to maintain consistency for the remainder of this study, ΔH^0_1 (also referred to as ΔH^0) is used in the solubility model given by Equation (3). The mechanism of N_2 dissolution is the same for both high H_2O and low H_2O slab-melts. Hence, similar to high H_2O slab-melts, low H_2O slab-melts are also not expected to show any correlation between $\ln(K)$ and $1/T$. The ΔH^0 of low and high H_2O slab-melts are calculated as −48.2(±1.2) kJ/mol and −58.7(±4.4) kJ/mol, respectively.

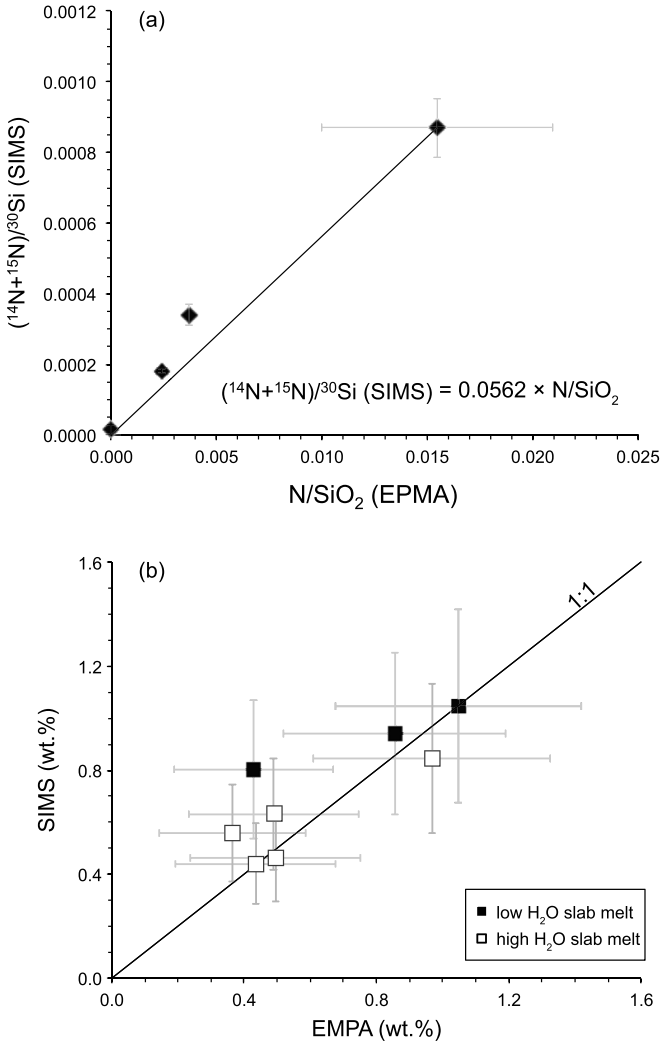

Fig. 2. (a) Calibration curve for SIMS analyses. The most nitrogen-rich glass (A875) is selected as the primary calibrant, and using the relative sensitivity factor defined by A875, the nitrogen contents of the two other calibration materials (HP-15 and HP-16) are calculated. The uncertainty estimate for EPMA analyses arises from repeatability and that of SIMS analyses from heterogeneity in the glasses. For further explanation, see text in Supplementary Information. (b) Nitrogen concentration in slab melts measured using EMPA versus SIMS. The uncertainty estimates for EPMA analyses arise from repeatability and that of SIMS analyses from heterogeneity in the glasses.

4. Discussion

4.1. Comparison of the solubility model from this study with earlier studies

We tested the solubility model from this study on synthetic haplogranitic compositions with 11–13 wt.% H_2O produced at 0.2 and 1 GPa, 800 °C, and $fO_2 \sim$ NNO (Ni–NiO buffer) (Li et al., 2015), nominally anhydrous Na_2O–$4SiO_2$ compositions produced at 1–2 GPa, 1600 °C (Roskosz et al., 2006) and

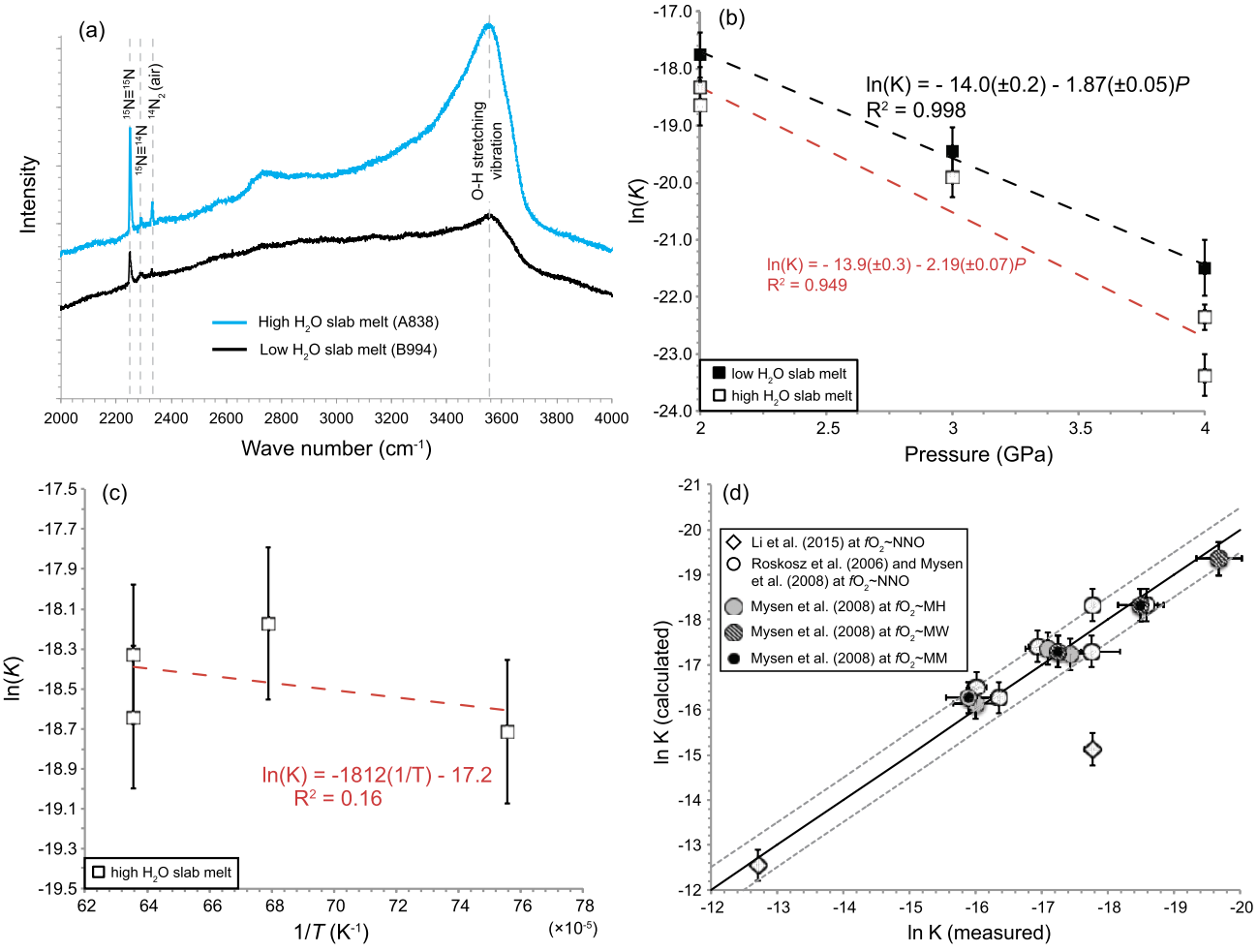

Fig. 3. (a) Raman spectra of two representative samples from high H_2O and low H_2O slab-melts showing peaks corresponding to molecular N_2 with different isotopic combinations. The spectra have not been corrected for atmospheric N. See Supplementary Information for further details. (b) Equilibrium constant K ($X_{N_2}^{melt}/f_{N_2}^{fluid}$) versus pressure for low H_2O and high H_2O slab-melts (this study). K was calculated for the melt compositions using dissolved N_2 concentration in the glasses and estimated respective fluid compositions (see text for details). Regression of K values for slab-melts from this study (black line for low H_2O slab-melt, red line for high H_2O slab-melt) produced the following parameters: ln $K^0 = -14.0$ (±0.2), $\Delta V^0 = 24.1$ (±0.6) $cm^3\,mol^{-1}$ for low H_2O slab-melt; ln $K^0 = -13.9$ (±0.3), $\Delta V^0 = 28.2$ (±0.9) $cm^3\,mol^{-1}$ for high H_2O slab-melt. (c) Equilibrium constant K ($X_{N_2}^{melt}/f_{N_2}^{fluid}$) versus reciprocal temperature for high H_2O slab-melts (this study). Given the poor correlation between ln(K) and $1/T$ ($R^2 = 0.16$) for high H_2O slab-melts, the slope of the best-fit line can be considered zero for practical purposes. This produces $\Delta H_1^0 = -56.5$ (±1.7) $kJ\,mol^{-1}$ and $\Delta H_2^0 = -58.7$ (±4.4) $kJ\,mol^{-1}$ (see text for details) for high H_2O slab-melts. Similarly, ΔH_1^0 for low H_2O slab-melts is −48.2 (±1.2) kJ/mol (see text for details). (d) Comparison of equilibrium constants estimated from experiments in previous studies (ln K measured) and from solubility model, equation (3) (ln K calculated). The solid black line represents 1:1 correlation, and the broken lines represent a 0.5 log unit departure from the 1:1 line. (For interpretation of the references to colour in this figure legend, the reader is referred to the web version of this article.)

1–2.5 GPa, 1300–1500 °C (Mysen et al., 2008), at fO_2 imposed by MH (Fe_3O_4–Fe_2O_3), MM (MnO–Mn_3O_4), NNO (Ni–NiO) and MW (FeO–Fe_3O_4) buffers in the order of decreasing oxygen fugacity (Fig. 3d). Calculated on an anhydrous basis, Na_2O–$4SiO_2$ melts have higher non-bridging oxygen per tetrahedrally co-ordinated cation or NBO/T (0.5), meaning a higher ionic porosity, as compared to the NBO/T of slab-melts from this study (0.02) and the haplogranites (0.01). Although there is no available quantification of NBO/T (or ionic porosity) of silicate melts with H_2O speciation, it can be qualitatively concluded that the hydrous slab-melts from this study and the hydrous haplogranites have higher NBO/T than what has been calculated for them on an anhydrous basis, due to the presence of OH^- in the former. Perhaps within uncertainty, the hydrous melts from this study and the haplogranites have similar NBO/T as the nominally anhydrous Na_2O–$4SiO_2$ melts, leading to applicability of the N solubility model on the latter melt compositions.

Our model can reproduce the N solubility obtained from previous studies within 0.5 log units (further details are included in Supplementary Information). The only outlier in solubility prediction is the hydrous haplogranite produced at 1 GPa, 800 °C (Li et al., 2015), where the calculated solubility is 2.6 log units away from the measured solubility. Although difficult to pinpoint, one of the reasons for the discrepancy could be an underestimation of the dissolved N_2 content in the experiment. Thus this solubility model can be used to predict N solubility of slab-melts at P–T–fO_2 conditions applicable for subduction zones. We used the solubility model to constrain the maximum amount of N that can be transported away by slab-derived melts from the subducted slab to the arc source.

4.2. Approach to quantification of recycling efficiency of N across modern day subduction zones

The following sub-sections describe the steps we have employed to constrain the recycling efficiency of N in modern-day subduction zones.

4.2.1. Assumptions in constraining recycling efficiency of N

While all slabs undergo thermally driven dehydration associated with subduction, hot to intermediate slabs (as defined in this study) also undergo partial melting induced by fluid flux from the dehydration of the underlying altered peridotite (Walowski et al., 2015) or due to the diapiric rise of a mélange comprised of a physical mixture of sediments and basalt from the slab-top towards the hotter core of the mantle-wedge (Nielsen and Marschall, 2017). Consequently, cold slabs undergo dehydration only. Here, we considered the dehydration and/or melting of sediments and basalt (extrusives and sheeted dikes) and excluded gabbros underlying the basaltic section. Gabbros are heated enough to dehydrate and/or melt in the hottest subduction zones (van Keken et al., 2011). In the cases of Mexico and Cascadia, the two hottest subduction zones today (based on slab top temperatures at 100 km depth), the slab Moho *P–T* path intersects the wet solidus of basalt, meaning that a sufficient fluid flux from the underlying serpentinite can sustain melting (van Keken et al., 2011). For the remaining hot to intermediate subduction zones, the assumption that the gabbro does not dehydrate (hence does not release N), is an end-member scenario. Therefore, it should be noted that the N recycling efficiency (percentage of incoming N sent to the deep mantle beyond the arc filter) determined in this study is an upper limit. Although studies have demonstrated the role of a diapiric rise of mélange in subduction zones (Nielsen and Marschall, 2017), an evaluation of the effect of diapirs on thermal structures of subduction zones remains to be constrained. In this study we have not included the role of diapirs on N transfer from the subducted slab to the arc source.

4.2.2. Quantify N input in present-day subduction zones

In order to constrain the modern-day net subduction rate of N, the first step is to estimate the net influx of N across all subduction zones. We took into account 55 subduction zone segments (Syracuse et al., 2010; van Keken et al., 2011) (Supplementary Table 1) and calculated the mass of subducting sediment in each arc segment from the convergence velocity, length of each arc segment, sediment thickness and sediment density. Following a previous study (Hacker, 2008), we assumed the sediment to be underlain by a 7 km thick oceanic crust, consisting of 600 m of extrusives, 1.4 km of sheeted dikes and 5 km of gabbro. The densities of oceanic crust are also from (Jarrard, 2003). As a first approximation, given their altered mineralogy, we assumed that the density of extrusives is a mixture of 80% saponite and 20% celadonite (Jarrard, 2003). From this we calculate the total mass of subducted N using the N concentrations of sediments (424 ± 33 μg/g), basalts (extrusives and sheeted dikes; 6.5 ± 2.6 μg/g) and gabbro (5.9 ± 3.0 μg/g) (Busigny et al., 2011). N concentration in serpentinized mantle was set to 4.5 μg/g (Halama et al., 2014), but the extent of serpentinization of the lithospheric mantle, the mechanism of N incorporation in serpentinite and the pathway for its release during dehydration are poorly known (Halama et al., 2014). Hence, we ignored N influx or release from serpentinite in this study.

4.2.3. Quantify N carried away from the slab by aqueous fluids

We constrained N transport by aqueous fluids in subduction zones using the model of Li and Keppler (2014) with the following equations (Equations (5) and (7) in Li and Keppler, 2014):

$$K = \frac{X_{NH_3}^2}{X_{N_2}} \tag{4}$$

$$\log K = -9.694 + \frac{8272}{T} + 0.0211 \times P - 0.8020 \times \Delta\text{NNO} \tag{5}$$

where, X = mole fraction of NH_3 or NH^{4+} and N_2 species in the aqueous fluid, P = pressure in kbar, T = temperature in Kelvin, ΔNNO = log unit deviation of oxygen fugacity from Ni–NiO buffer. The above model does not take into account the effect of pH of the system (Mikhail et al., 2017; Mikhail and Sverjensky, 2014), meaning that we have not distinguished between molecular $NH_3{}^0$ and $NH_4{}^+$. Also, $NH_4{}^+$ versus $NH_3{}^0$ as the N-species in the aqueous fluid would not affect the overall N transport because both species carry one mole of N with them. We used equations (4) and (5) in conjunction with (i) the mass ratio of aqueous fluid and K-bearing minerals (estimated as mentioned in Supplementary Information), (ii) the partition coefficient of N between aqueous fluid and K-bearing minerals, and (iii) the oxygen fugacity of $\Delta NNO = 0$ needed to estimate both the concentration of N transferred to aqueous fluids and the concentration of N remaining in subducted slabs after fluid release along P–T trajectories (model D80 of Syracuse et al., 2010).

Due to the very similar ionic radii of $NH_4{}^+$ (the species of N incorporation in K-minerals in subducted slabs) and Rb^+ as well as their trace abundances in subduction zone systems, $NH_4{}^+$ can be modelled to closely follow the behaviour of Rb^+ (Shannon, 1976; Watenphul et al., 2009). This is also substantiated by independent studies estimating that approximately 20% of the influx of both N (Busigny et al., 2011) and Rb (Porter and White, 2009) in subduction zones is subsequently released via arc volcanism, assuming that the entire mass of these elements expelled from the slab is incorporated in arc volcanism. Partition coefficients of fluid/amphibole (19) and fluid/mica (0.1) from Adam et al. (2014) have been used.

4.2.4. Quantify N carried away from the slab by partial melt

Based on our experiments we conclude that at fO_2 conditions appropriate for subduction zones N is dissolved as molecular N_2 in the slab partial melt. As mentioned earlier in the introduction section, we have quantified the rate of N transported by slab-melts using two approaches, assuming – (i) N is dissolved in the slab-melt at its solubility limit, which anchors the highest (most efficient) rate of N removal from the slab, and (ii) N partitioning between the slab and slab-melt is controlled by $NH_4{}^+$, and $NH_4{}^+$ behaves similarly as Rb^+ due to having the same charge and similar ionic radii; hence, the behaviour of Rb^+ was used as a guide to the partitioning of N between the key N hosting minerals in the slab and any associated partial melt. $NH_4{}^+$ in the slab-minerals would convert to N_2 in the slab-melt, implying that the transfer of N from the slab to the slab-melt would be intermediate between N transport as molecular N_2 by solubility in slab-melt and N partitioning as $NH_4{}^+$ between both the slab and its partial melt. However, using approaches (i) and (ii) help bracket N transfer from the slab to the slab-melt between the upper and lower limits. The approaches used in the aforementioned two methods are described below.

The solubility limit of N in slab-melts was experimentally determined using the approach described above. The rate of N transfer from the slab at its solubility limit was estimated by combining the model given by Equation (3) and the degree of slab partial melting (calculated as described in Supplementary Information).

We calculated the amount of N partitioning into the slab-melt and the residual N in the slab using the non-modal batch melting equation (Shaw, 1970) as follows:

$$C_L = \frac{C_0}{F(1-P) + D_0} \tag{6}$$

$$C_S = C_L \times \frac{D_0 - PF}{1 - F} \tag{7}$$

where, C_L = concentration of N in slab-melt; C_0 = concentration of N in the slab after dehydration, prior to commencement of

melting; F = degree of slab partial melting; P = melting mode; D_0 = bulk partition coefficient, prior to commencement of melting.

The degree of slab partial melting was calculated as described in the Supplementary Information. N is mainly hosted by phengite in sediments and basalts (extrusives and sheeted dikes) and by amphibole in basalt. However, when melting commences in the slab, amphibole is already beyond its stability limit, hence, during melting, phengite is the only N hosting phase in both sediments and basalt.

$$D_0 = X_{phengite} \times K_d^{phengite/melt} \quad (8)$$

$X_{phengite}$ = modal proportion of phengite prior to onset of melting but after release of aqueous fluids (calculated by dividing the mass of phengite in sediments and basalt by the mass of sediments and basalt in the slab).

The partition coefficient of N (K_d) in phengite is similar to that of Rb, given NH_4^+ and Rb^+ have very close ionic radii. $K_d^{phengite/melt}$ varies from 1 to 10 (from https://earthref.org/KDD), hence, both partition coefficients values have been used to bracket the N transfer from the slab to its melt.

$$P = p^{phengite/melt} \times K_d^{phengite/melt} \quad (9)$$

$p^{phengite/melt}$ is estimated from the sediment partial melting study of Skora and Blundy (2010).

4.2.5. Release of aqueous fluids post-melting until 240 km

In all subduction zone segments, except Cascadia and Mexico, due to the curvature of the slab top P–T path past the zone of slab melting, the slab top becomes colder than the wet solidus of the slab. Hence, the slab top once again enters the zone of release of aqueous fluids by dehydration of hydrous minerals, provided that the hydrous minerals carrying both H_2O and N survive to these depths. While Mexico and Cascadia lose all H_2O (hence, N as well) beyond 100 km depth, these subduction zones do not go through the late stage of dehydration. We modelled N loss from the slab beyond the zone of melting until the depth of 240 km using equations (4) and (5), along with the mass ratio of aqueous fluid and K-bearing minerals, and partition coefficient of N between aqueous fluid and K-bearing minerals, at oxygen fugacity equivalent to that of the Ni–NiO buffer.

4.3. Recycling efficiency of N across modern day subduction zones

The "hot" slabs of Mexico and Cascadia dehydrate completely by 100 km depth (van Keken et al., 2011). This means by the time the slab exits the arc filter window beyond 100 km depth, N is completely expelled to the arc source. In contrast, more intermediate-temperature subduction zones, where slabs partially melt in addition to dehydrating, recycling efficiency ranges from 10% in Nicaragua to 87% in New Britain (Fig. 4a, Supplementary Tables 3–5). In cold subduction zones, where aqueous fluids are released but where no slab-melting occurs, recycling efficiency is overall higher than in hot to intermediate subduction zones; it varies between 69% in Tonga to 91% in Calabria (Fig. 4a, Supplementary Table 6). If N transfer to the arc source from the upper-slab is considered (sediments and basalt only), N transfer within hot to intermediate subduction zones will remove N completely, while up to 85% of N can be left behind if N is carried away from the slab by high H_2O slab-melt at $K_d^{phengite/melt} = 10$, as observed in New Britain (Fig. 4b, Supplementary Table 5). The dehydration of the upper-slab within cold subduction zones retains 51% of the N in Tonga to 90% in Calabria (Fig. 4b, Supplementary Table 6). The capacity of slab-melts to remove N from the subducting slab depends on the mechanism of N transfer to the melt phase, with transfer at solubility limit removing up to 93% of the slab N (estimate includes gabbro; Fig. 5a). Efficiency of N transfer by partitioning between the slab and the melt phase is directly correlated to (i) the degree of slab melting (Fig. 5b); and (ii) $K_d^{phengite/melt}$ during slab partial melting (a higher K_d retains more N in the slab; Fig. 5).

Globally today, 48–77% of subducted N passes through the arc filter and enters the deep mantle (Fig. 4a, Supplementary Tables 3–6). As a corollary, 23–52% of the N initially contained in the slab is released through a combination of aqueous fluids and slab-melts. This also implies that 0–38% of the N released from the slab is not degassed at arc volcanoes (comparing with arc outgassing estimates from Hilton et al., 2002; Supplementary Tables 3–5). The 0% deficit between the amount of N released from the slab versus N degassed at arcs comes from the recycling efficiency of 77%, the latter being an upper-limit of N retention to the deep mantle. Hence, a finite amount of N (up to 1.7×10^{11} g/yr, or 19% of the influx of N) will be sequestered in the mantle-wedge, or more likely in the lithosphere and lower crust of the overriding plate. This flux of N can either form a separate long-term reservoir, or could be part of the N recycled back to the deep mantle, depending on the stability of the lower crust and lithosphere in the overlying plate. Future studies should investigate the role of such reservoirs within the long-term cycling of N through the deep Earth. Taking into consideration N degassing at mid-ocean ridges (Hilton et al., 2002), intraplate settings and back-arc basins (Sano et al., 2001), 45–74% of N subducted enters the deep mantle at present.

4.4. Proportion of recycled N in the present mantle and the isotopic composition of Earth's primitive mantle

The recycling efficiency determined for N in subduction zones can be used as a tool to estimate the proportion of present-day mantle N that has been brought in via subduction. Likewise, the recycling efficiency can be used to constrain the isotopic composition of the primitive mantle. Here we examine two end-member scenarios: (i) subduction, in some form, likely similar to that operating today, had initiated 4 billion years ago (based on the geochemistry and stratigraphy of a sequence of rocks from Nuvvuaqittuq supracrustal belt in northern Quebec, Canada which are very similar to the sequence found in the forearc of Izu–Bonin–Mariana today; Turner et al., 2014); (ii) subduction similar to the present day had initiated 3 billion years ago. The latter is based on the modelled continental growth rate decreasing from 3 billion years onwards, which is interpreted as representing the onset of subduction (Dhuime et al., 2012). Numerical models of thermochemical convection also show that subduction prior to 3 billion years was likely episodic, being mostly short-lived (Rozel et al., 2017). Additional support for the assumption that the present-day nitrogen recycling efficiency can be applied to the Archaean is discussed in the Supplementary Information.

Using the above constraints on the timing of modern-day subduction initiation, the N recycling rates constrained in this study, and the mass of N in the mantle today (Johnson and Goldblatt, 2015), we have estimated the mass of N in the Earth's mantle back in time until the initiation of modern-day plate tectonics. We find that the present-day mantle consists of $17 \pm 8\%$ of recycled N (if subduction was initiated 4 billion years ago) and $12 \pm 5\%$ (if subduction was initiated 3 billion years ago) (Fig. 6a). This implies that the isotopic composition of the Earth's primitive mantle would have differed from the present-day value of $\delta^{15}N \approx -5‰$ (Cartigny and Marty, 2013). Using our recycling rates for N and $\delta^{15}N = +6‰$ for subducted crust (Cartigny and Marty, 2013), we estimate the $\delta^{15}N$ of the Earth's original mantle to be $-6.8 \pm 0.9‰$ (if subduction initiated 4 billion years ago) and $-6.3 \pm 1.2‰$ (if subduction

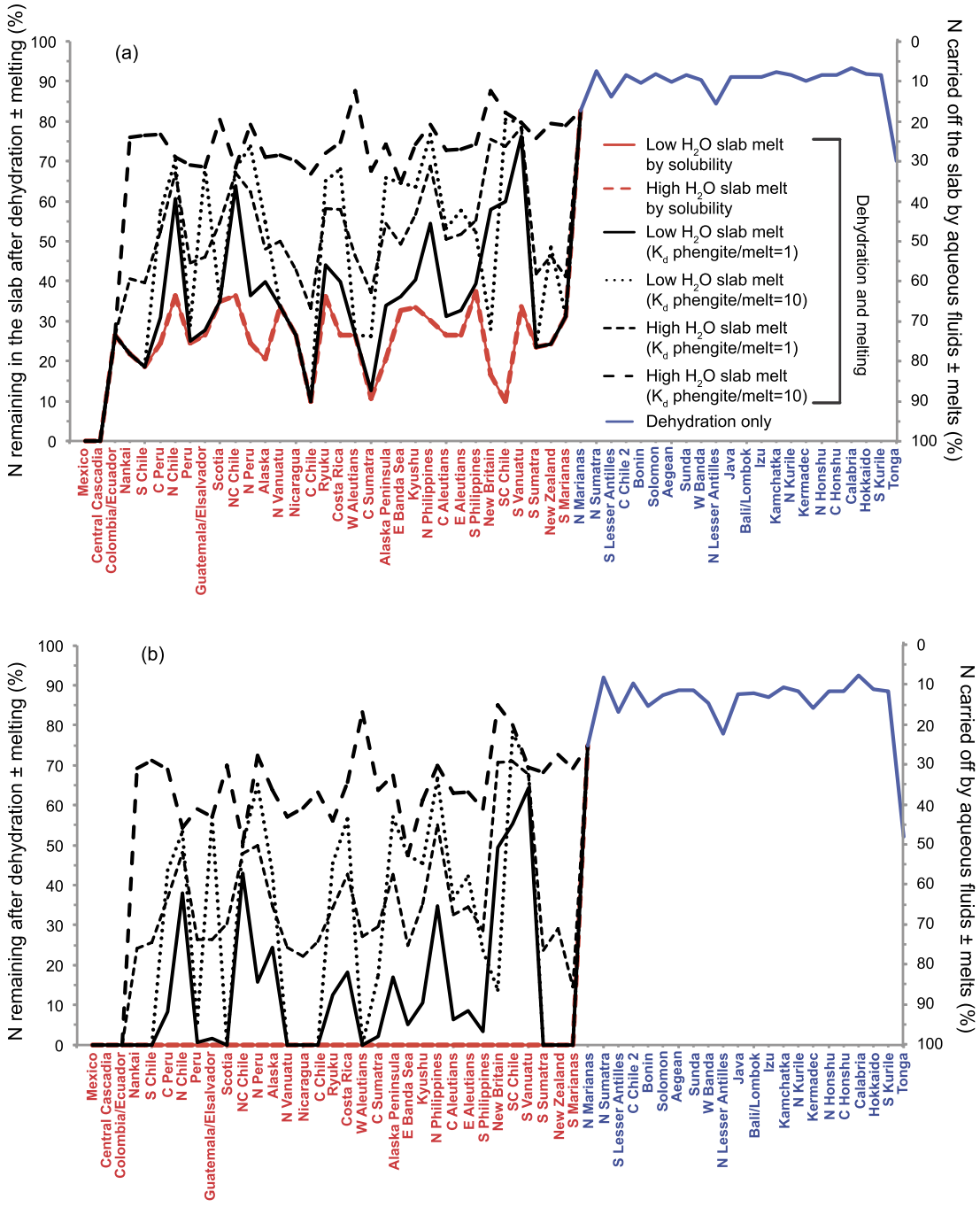

Fig. 4. (a) Percentage of N remaining in the total slab (sediments, extrusives and gabbro) or expelled, after its dehydration and partial melting. (b) Percentage of N remaining in the upper slab (sediments and extrusives only) or expelled after dehydration and partial melting of the subducted slab. The subduction zones are arranged with the slab-top temperatures at 100 km depth increasing towards the left (based on model D80 of Syracuse et al., 2010). Subduction zones in red both dehydrate and partially melt, while, subduction zones to the right only dehydrate. (For interpretation of the references to colour in this figure legend, the reader is referred to the web version of this article.)

initiated 3 billion years ago) (Fig. 6b). These isotopic compositions lie within the range shown by peridotitic Archaean diamonds (Cartigny and Marty, 2013). The departure in isotopic composition of the primitive mantle from the −5‰ in the present-day mantle implies that there is a discernible secular shift. Accordingly, the extreme values for δ^{15}N of −25‰ suggested for primitive mantle (Javoy, 1997) and −40‰ found in two Archaean diamonds (Cartigny and Marty, 2013) either represent a heterogeneous primitive mantle (Palot et al., 2012) or are the by-products of isotope fractionation during the metasomatic origin of diamonds (Cartigny, 2005). Future studies constraining the nature and proportion of contribution of parent bodies of the Earth should take into account the revised primitive mantle isotopic composition.

4.5. Nitrogen in the Archaean atmosphere and implications for Archaean climate

The rate of N drawdown from the atmosphere, given by the rate of N fixation in the crust, can be used to extrapolate the N content of the Archaean atmosphere. As discussed in the Supplementary Information, the rate of N fixation in the crust during the Hadean was of an equal order of magnitude to the present-day rate of N

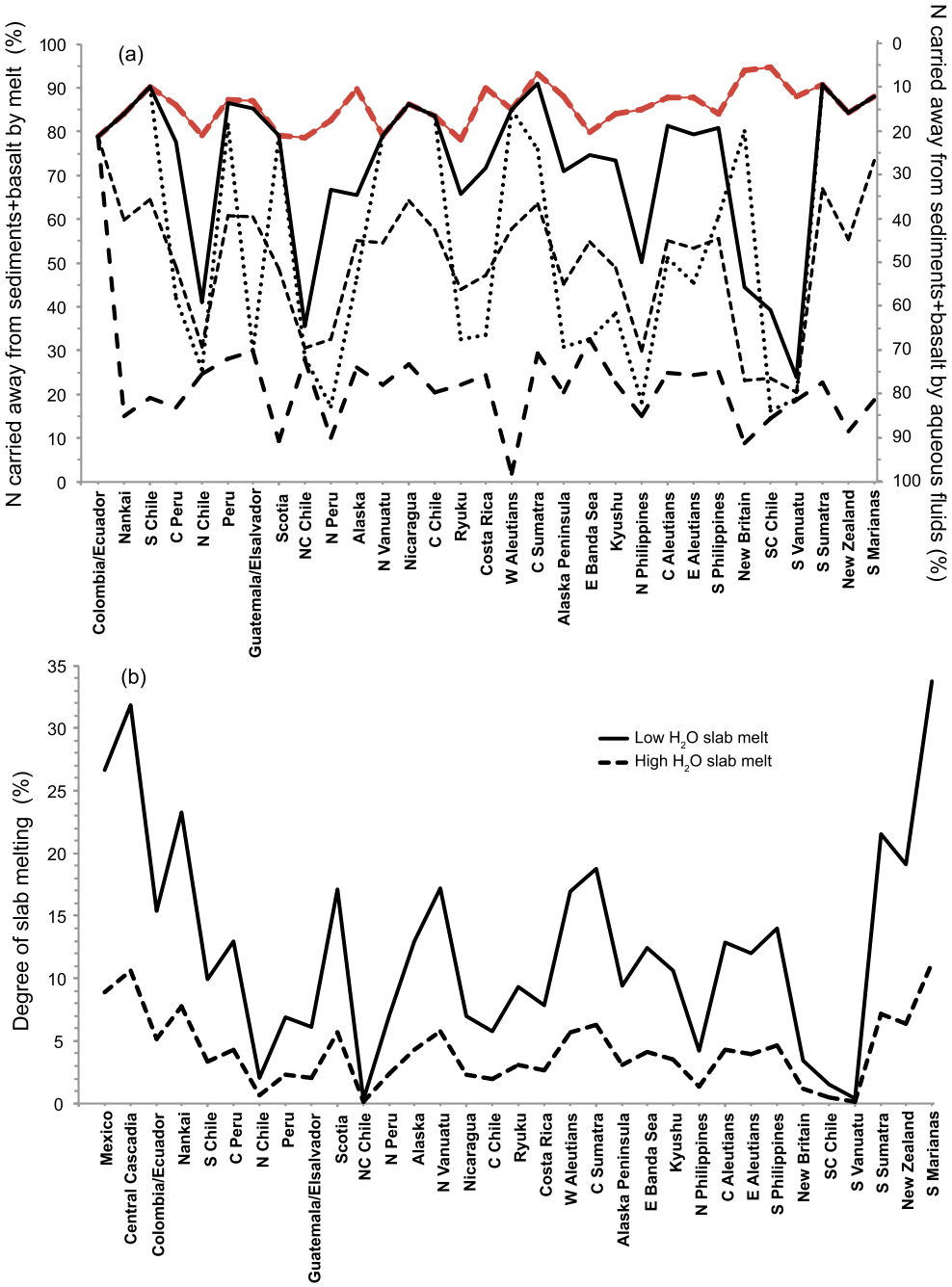

Fig. 5. (a) Percentage of incoming N expelled from the subducted slab by partial melt and by aqueous fluids in hot to intermediate subduction zones that undergo both dehydration and partial melting of the slab. The curves are the same as Fig. 4. (b) Degree of slab melting in hot to intermediate subduction zones (see Supplementary Information on how it was calculated). The subduction zones are arranged with the slab-top temperatures at 100 km depth (based on model D80 of Syracuse et al., 2010) increasing towards the left.

transfer from the crust to the mantle via subduction. On the other hand, today's rate of N fixation in the crust is 2 orders of magnitude higher than the present-day rate of N transfer from the crust to the mantle via subduction (references in Supplementary Information). Hence, using the rate of N subduction from the crust to the mantle would provide a lower limit to the rate of N drawdown from the atmosphere to the crust. Consequently, the mass of N in the Archaean atmosphere calculated using present-day subduction rates must represent a lower limit.

To estimate the mass of N in the Archaean atmosphere 3 and 4 billion years ago, we subtracted the net degassing flux of N from arcs and back-arc basins (Hilton et al., 2002), mid-ocean ridges and intraplate-settings (Sano et al., 2001) from the influx of N at subduction zones today (Supplementary Table 1). This yields 1.4 ± 0.1 and 1.6 ± 0.2 times PAN (present-day atmospheric nitrogen) in the atmosphere at 3 and 4 billion years ago, respectively (Fig. 6c). Our result of higher N mass in the Archaean atmosphere, estimated by an independent approach, contradicts estimates of lower Archaean atmospheric total pressures and N_2 partial pressures (Marty et al., 2013; Som et al., 2016, 2012); but corroborates the results of two recent studies (Barry and Hilton, 2016; Busigny et al., 2003). In fact, a recent study (Kavanagh and Goldblatt, 2015) viewed critically the paleopycnometer of Som et al. (2012) that is based on fossil raindrop size distribution. They concluded that such an approach under-estimates the Archaean atmospheric density. A higher partial pressure (i.e. higher atmospheric

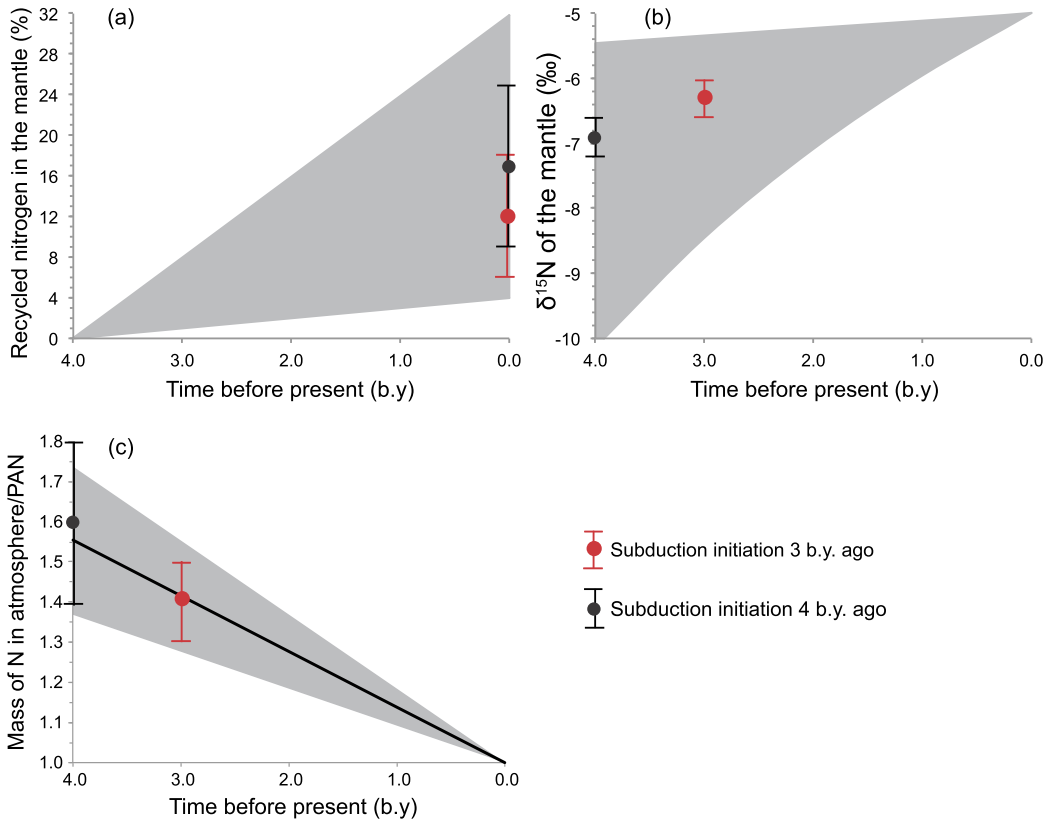

Fig. 6. (a) Percentage of N recycled to the deep mantle since 4 billion years ago. The grey area covers the range due to the lowest and highest N recycling efficiencies. (b) δ^{15}N of the mantle calculated from the present to 4 billion years ago. The grey area represents the range in isotopic composition estimated by the lowest and highest N recycling efficiencies. (c) Mass of N in the atmosphere versus time, normalized to PAN (present-day atmospheric nitrogen). The grey area arises from uncertainties in estimates of N flux entering subduction zones today, as reported in Supplementary Table 1.

mass) of N in the Archaean would have induced warming of the early Earth by pressure broadening the absorption lines of greenhouse gases, thereby increasing their potency (Goldblatt et al., 2009). This could account for the relatively warm temperatures present at the Earth's surface during the Archaean, which seem inconsistent with the faint young Sun which would have been present at the time. The net transfer of N from the atmosphere to the mantle through geologic time requires a higher N mass in the Archaean atmosphere, thereby increasing the atmospheric pressure and partial pressure of N_2. According to the model from a recent study (Goldblatt et al., 2009), 1.4–1.6 times PAN in the Archaean atmosphere yields surface temperatures around 8–10 °C at $pCO_2 = 10^{-2}$ bar (based on 2.2 billion year old paleosol data of Sheldon, 2006). A higher pCO_2, expected in the atmosphere 3 to 4 billion years ago (Navarro-Gonzalez et al., 2001), would further enhance warming of surface temperatures and suppressing glaciation despite the condition of a faint young Sun.

5. Conclusion

Nitrogen recycling efficiency, or the proportion of subducted nitrogen that escapes slab dehydration and/or melting and ultimately enters the deep Earth – determines (a) if nitrogen in the present-day mantle is of primordial (i.e. inherited from accretion and magma-ocean crystallization) or recycled (i.e. introduced via subduction) origin. Furthermore, recycling efficiency provides direct information on whether the Archaean atmosphere had a higher N partial pressure than the present, having major implications for Archaean climate. Here we employed a novel forward approach for estimating present-day nitrogen recycling efficiency. We quantified the efficiency of nitrogen transfer via both aqueous fluids and slab partial melts, from the subducted slab to the sub-arc mantle across subduction zones of various thermal regimes. We experimentally constrained the solubility limits of nitrogen in slab partial melts to estimate the lower limit for nitrogen retention of the deep subducted slab. Globally, 45–74% of subducted nitrogen enters the deep mantle. Using this recycling efficiency, we determined that only 12±5% to 17±8% of nitrogen in the present-day mantle is of recycled origin and that the Archaean atmosphere had at least 1.4–1.6 times higher nitrogen mass than today, which would have helped warm Earth's surface above freezing despite a faint young Sun.

Acknowledgements

The authors would like to thank Hans Keppler, Marc Hirschmann, Katie Kelley, Rajdeep Dasgupta, Gregor Golabek, and Pranabendu Moitra for helpful discussions; Sami Mikhail and an anonymous reviewer for their detailed and constructive comments; Richard Katz for bringing to our attention the study by Wordsworth and Pierrehumbert (2014); Tariq Ejaz for assisting with synthesis of the blank glass and equal isotope glass for SIMS calibration; Hubert Schulze, Raphael Njul, Heinz Fischer and Stefan Übelhack for technical assistance; Detlef Krauße for assistance with the electron microprobe; and Frédéric Couffignal for his support of the SIMS analyses. This work received financial support from the Visiting Scientist Program at Bayerisches Geoinstitut and the Alexander von Humboldt Postdoctoral fellowship to A.M., and from the NSFC (41673064) to Y.L.

Appendix A. Supplementary material

Supplementary material related to this article can be found online at https://doi.org/10.1016/j.epsl.2017.11.045.

References

Adam, J., Locmelis, M., Afonso, J.C., Rushmer, T., Fiorentini, M.L., 2014. The capacity of hydrous fluids to transport and fractionate incompatible elements and metals within the Earth's mantle. Geochem. Geophys. Geosyst. 15, 2241–2253. https://doi.org/10.1002/2013GC005199.

Barry, P., Hilton, D., 2016. Release of subducted sedimentary nitrogen throughout Earth's mantle. Geochem. Perspect. Lett. 2, 148–158.

Busigny, V., Cartigny, P., Philippot, P., 2011. Nitrogen isotopes in ophiolitic metagabbros: a re-evaluation of modern nitrogen fluxes in subduction zones and implication for the early Earth atmosphere. Geochim. Cosmochim. Acta 75, 7502–7521. https://doi.org/10.1016/j.gca.2011.09.049.

Busigny, V., Cartigny, P., Philippot, P., Ader, M., Javoy, M., 2003. Massive recycling of nitrogen and other fluid-mobile elements (K, Rb, Cs, H) in a cold slab environment: evidence from HP to UHP oceanic metasediments of the Schistes Lustrés nappe (western Alps, Europe). Earth Planet. Sci. Lett. 215, 27–42. https://doi.org/10.1016/S0012-821X(03)00453-9.

Carroll, M.R., Stolper, E.M., 1993. Noble gas solubilities in silicate melts and glasses: new experimental results for argon and the relationship between solubility and ionic porosity. Geochim. Cosmochim. Acta 57, 5039–5051. https://doi.org/10.1016/0016-7037(93)90606-W.

Cartigny, P., 2005. Stable isotopes and the origin of diamond. Elements 1, 79–84. https://doi.org/10.2113/gselements.1.2.79.

Cartigny, P., Marty, B., 2013. Nitrogen isotopes and mantle geodynamics: the emergence of life and the atmosphere–crust–mantle connection. Elements 9, 359–366. https://doi.org/10.2113/gselements.9.5.359.

Dhuime, B., Hawkesworth, C.J., Cawood, P.A., Storey, C.D., 2012. A change in the geodynamics of continental growth 3 billion years ago. Science 335, 1334–1336. https://doi.org/10.1126/science.1216066.

Fischer, T.P., Hilton, D.R., Zimmer, M.M., Shaw, A.M., Sharp, Z.D., Walker, J.A., 2002. Subduction and recycling of nitrogen along the central American margin. Science 297, 1154–1157. https://doi.org/10.1126/science.1073995.

Goldblatt, C., Claire, M.W., Lenton, T.M., Matthews, A.J., Watson, A.J., Zahnle, K.J., 2009. Nitrogen-enhanced greenhouse warming on early Earth. Nat. Geosci. 2, 891–896.

Hacker, B.R., 2008. H_2O subduction beyond arcs. Geochem. Geophys. Geosyst. 9. https://doi.org/10.1029/2007GC001707.

Halama, R., Bebout, G., John, T., Scambelluri, M., 2014. Nitrogen recycling in subducted mantle rocks and implications for the global nitrogen cycle. Int. J. Earth Sci. 103, 2081–2099. https://doi.org/10.1007/s00531-012-0782-3.

Hilton, D.R., Fischer, T.P., Marty, B., 2002. Noble gases and volatile recycling at subduction zones. Rev. Mineral. Geochem. 47, 319–370. https://doi.org/10.2138/rmg.2002.47.9.

Hirschmann, M.M., Withers, A.C., Ardia, P., Foley, N.T., 2012. Solubility of molecular hydrogen in silicate melts and consequences for volatile evolution of terrestrial planets. Earth Planet. Sci. Lett. 345–348, 38–48. https://doi.org/10.1016/j.epsl.2012.06.031.

Jarrard, R.D., 2003. Subduction fluxes of water, carbon dioxide, chlorine, and potassium. Geochem. Geophys. Geosyst. 4. https://doi.org/10.1029/2002GC000392.

Javoy, M., 1997. The major volatile elements of the Earth: their origin, behavior, and fate. Geophys. Res. Lett. 24, 177–180. https://doi.org/10.1029/96GL03931.

Johnson, B., Goldblatt, C., 2015. The nitrogen budget of Earth. Earth-Sci. Rev. 148, 150–173. https://doi.org/10.1016/j.earscirev.2015.05.006.

Kavanagh, L., Goldblatt, C., 2015. Using raindrops to constrain past atmospheric density. Earth Planet. Sci. Lett. 413, 51–58. https://doi.org/10.1016/j.epsl.2014.12.032.

Kawamoto, T., Yoshikawa, M., Kumagai, Y., Mirabueno, M.H.T., Okuno, M., Kobayashi, T., 2013. Mantle wedge infiltrated with saline fluids from dehydration and decarbonation of subducting slab. Proc. Natl. Acad. Sci. USA 110, 9663–9668. https://doi.org/10.1073/pnas.1302040110.

Li, L., Bebout, G.E., 2005. Carbon and nitrogen geochemistry of sediments in the Central American convergent margin: insights regarding subduction input fluxes, diagenesis, and paleoproductivity. J. Geophys. Res., Solid Earth 110, B11202. https://doi.org/10.1029/2004JB003276.

Li, Y., Huang, R., Wiedenbeck, M., Keppler, H., 2015. Nitrogen distribution between aqueous fluids and silicate melts. Earth Planet. Sci. Lett. 411, 218–228. https://doi.org/10.1016/j.epsl.2014.11.050.

Li, Y., Keppler, H., 2014. Nitrogen speciation in mantle and crustal fluids. Geochim. Cosmochim. Acta 129, 13–32. https://doi.org/10.1016/j.gca.2013.12.031.

Li, Y., Marty, B., Shcheka, S., Zimmermann, L., Keppler, H., 2016. Nitrogen isotope fractionation during terrestrial core–mantle separation. Geochem. Perspect. Lett. 2, 138–147. https://doi.org/10.7185/geochemlet.1614.

Li, Y., Wiedenbeck, M., Shcheka, S., Keppler, H., 2013. Nitrogen solubility in upper mantle minerals. Earth Planet. Sci. Lett. 377–378, 311–323. https://doi.org/10.1016/j.epsl.2013.07.013.

Marty, B., Dauphas, N., 2003. The nitrogen record of crust–mantle interaction and mantle convection from Archean to Present. Earth Planet. Sci. Lett. 206, 397–410. https://doi.org/10.1016/S0012-821X(02)01108-1.

Marty, B., Zimmermann, L., Pujol, M., Burgess, R., Philippot, P., 2013. Nitrogen isotopic composition and density of the archean atmosphere. Science 342, 101–104. https://doi.org/10.1126/science.1240971.

Mikhail, S., Barry, P.H., Sverjensky, D.A., 2017. The relationship between mantle pH and the deep nitrogen cycle. Geochim. Cosmochim. Acta 209, 149–160. https://doi.org/10.1016/j.gca.2017.04.007.

Mikhail, S., Sverjensky, D.A., 2014. Nitrogen speciation in upper mantle fluids and the origin of Earth's nitrogen-rich atmosphere. Nat. Geosci. 7, 816–819. https://doi.org/10.1038/ngeo2271.

Mysen, B.O., Yamashita, S., Chertkova, N., 2008. Solubility and solution mechanisms of NOH volatiles in silicate melts at high pressure and temperature – amine groups and hydrogen fugacity. Am. Mineral. 93, 1760–1770.

Navarro-Gonzalez, R., McKay, C.P., Mvondo, D.N., 2001. A possible nitrogen crisis for Archaean life due to reduced nitrogen fixation by lightning. Nature 412, 61–64.

Nielsen, S.G., Marschall, H.R., 2017. Geochemical evidence for mélange melting in global arcs. Sci. Adv. 3. https://doi.org/10.1126/sciadv.1602402.

Palot, M., Cartigny, P., Harris, J.W., Kaminsky, F.V., Stachel, T., 2012. Evidence for deep mantle convection and primordial heterogeneity from nitrogen and carbon stable isotopes in diamond. Earth Planet. Sci. Lett. 357–358, 179–193. https://doi.org/10.1016/j.epsl.2012.09.015.

Paonita, A., 2005. Noble gas solubility in silicate melts: a review of experimentation and theory, and implications regarding magma degassing processes. Ann. Geophys..

Pirard, C., Hermann, J., 2015. Focused fluid transfer through the mantle above subduction zones. Geology 43, 915–918. https://doi.org/10.1130/g37026.1.

Porter, K.A., White, W.M., 2009. Deep mantle subduction flux. Geochem. Geophys. Geosyst. 10, Q12016. https://doi.org/10.1029/2009GC002656.

Roskosz, M., Mysen, B.O., Cody, G.D., 2006. Dual speciation of nitrogen in silicate melts at high pressure and temperature: an experimental study. Geochim. Cosmochim. Acta 70, 2902–2918.

Rozel, A.B., Golabek, G.J., Jain, C., Tackley, P.J., Gerya, T., 2017. Continental crust formation on early Earth controlled by intrusive magmatism. Nature 545, 332–335. https://doi.org/10.1038/nature22042.

Sano, Y., Takahata, N., Nishio, Y., Fischer, T.P., Williams, S.N., 2001. Volcanic flux of nitrogen from the Earth. Chem. Geol. 171, 263–271.

Shannon, R., 1976. Revised effective ionic radii and systematic studies of interatomic distances in halides and chalcogenides. Acta Crystallogr., Sect. A 32, 751–767. https://doi.org/10.1107/S0567739476001551.

Shaw, D.M., 1970. Trace element fractionation during anatexis. Geochim. Cosmochim. Acta 34, 237–243. https://doi.org/10.1016/0016-7037(70)90009-8.

Sheldon, N.D., 2006. Precambrian paleosols and atmospheric CO_2 levels. Precambrian Res. 147, 148–155. https://doi.org/10.1016/j.precamres.2006.02.004.

Skora, S., Blundy, J., 2010. High-pressure hydrous phase relations of radiolarian clay and implications for the involvement of subducted sediment in arc magmatism. J. Petrol. 51, 2211–2243. https://doi.org/10.1093/petrology/egq054.

Som, S.M., Buick, R., Hagadorn, J.W., Blake, T.S., Perreault, J.M., Harnmeijer, J.P., Catling, D.C., 2016. Earth's air pressure 2.7 billion years ago constrained to less than half of modern levels. Nat. Geosci. 9, 448–451. https://doi.org/10.1038/ngeo2713.

Som, S.M., Catling, D.C., Harnmeijer, J.P., Polivka, P.M., Buick, R., 2012. Air density 2.7 billion years ago limited to less than twice modern levels by fossil raindrop imprints. Nature 484, 359–362. https://doi.org/10.1038/nature10890.

Syracuse, E.M., van Keken, P.E., Abers, G.A., 2010. The global range of subduction zone thermal models. Phys. Earth Planet. Inter. 183, 73–90. https://doi.org/10.1016/j.pepi.2010.02.004.

Turner, S., Rushmer, T., Reagan, M., Moyen, J.-F., 2014. Heading down early on? Start of subduction on Earth. Geology 42, 139–142. https://doi.org/10.1130/g34886.1.

van Keken, P.E., Hacker, B.R., Syracuse, E.M., Abers, G.A., 2011. Subduction factory, 4: depth-dependent flux of H_2O from subducting slabs worldwide. J. Geophys. Res., Solid Earth 116. https://doi.org/10.1029/2010JB007922.

Walowski, K.J., Wallace, P.J., Hauri, E., Wada, I., Clynne, M.A., 2015. Slab melting beneath the Cascade Arc driven by dehydration of altered oceanic peridotite. Nat. Geosci. 8, 404.

Watenphul, A., Wunder, B., Heinrich, W., 2009. High-pressure ammonium-bearing silicates: implications for nitrogen and hydrogen storage in the Earth's mantle. Am. Mineral. 94, 283–292.

Wordsworth, R., Pierrehumbert, R., 2014. Abiotic oxygen-dominated atmospheres on terrestrial habitable zone planets. Astrophys. J. Lett. 785, L20.